33rd Annual International Conference of the IEEE EMBS
Boston, Massachusetts USA, August 30 - September 3, 2011

Delivering Optical Power to Subcutaneous Implanted Devices

Sahar Ayazian, *Student Member*, and Arjang Hassibi, *Member, IEEE*

Abstract— **In this paper, a new, easy-to-implement, and MRI-compatible approach for delivering power to implantable devices is presented. The idea is to harvest the energy of light within the *therapeutic window* wavelengths, where the optical absorption is small, by using subcutaneous photovoltaic (PV) cells. Depending on the application, this energy can then be used to directly drive the embedded electronics of an implanted device or recharge its battery. To show the feasibility of this system, a CMOS chip based on this concept has been implemented and tested. The experimental results demonstrate that μW's of power in ambient light conditions can be harvested using mm^2-size PV cells. This amount of power is sufficient to address the needs of many low-power applications.**

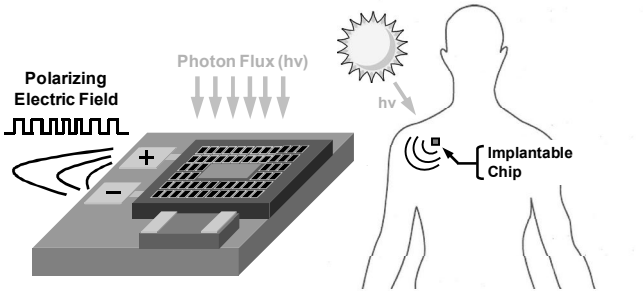

Fig. 1. The proposed method to deliver power a subcutaneous implanted device.

I. Introduction

The progress in the semiconductor industry has significantly contributed to the healthcare and life sciences industries. Specifically, implantable devices have benefitted from the continuous growth in the semiconductor field and advances of VLSI fabrication processes. Many of the design challenges in the implantable devices such as sensing, ability to make autonomous decisions, or connecting wirelessly to outside, have been addressed by the downsizing of the circuit structure, advances in packaging technologies, and other related works [1].

The issue of providing energy for implantable devices is still a big challenge. This is despite the recent improvements in that field. It is imperative to realize that the more power is available and the longer it lasts directly affects the capabilities of that device and its *in-vivo* "life-time".

In the past few decades, various methods have been proposed to provide energy for implanted devices. Some of the methods have been successfully reduced to practice and a couple of them have been even commercialized. The most common approach is to use high-capacity batteries to provide the required energy [2-3]. In low-power applications (e.g., pacemaker [4]) this battery can successfully run the device for 8 to 12 years and then be replaced afterwards through surgery. Chemical leakage of *in-vivo* batteries can potentially be harmful to the body [5], but by designing proper packages, any potential risks have been mitigated.

An alternative approach is to create *wireless* techniques by which one can recharge this battery (or any other implanted energy storage element) to prolong the life-time of the device. Inductive coupling (*i.e.*, near-field coupling) is one technique which can do this. However, proper alignment of the transmitting coil and the *in-vivo* receiving coil is critical for efficient power delivery [6-8]. Far-field coupling of two antennae to deliver power has also been demonstrated [9]. This approach results in smaller size devices (i.e., receiving antennae) in the expense of higher tissue loss [10-11]. The directivity of the transmitting antenna is also critical in this approach with directional alignment requirements somewhat similar to the inductive-coupling approach. In both methods the total harvested power is proportional to the size (area) of the receiving element. This fundamentally limits the upper bound of the delivered power for cm^3-size implanted devices. Moreover, the necessity of *in-vivo* coils or antennas in such devices makes them inherently MRI-incompatible.

In this paper, a new, easy-to-implement and MRI-compatible method for delivering power to implanted devices is presented. The basic idea is to harvest the energy of the ambient light passing through the tissue and run the subcutaneous (below the skin) implanted device (see Fig. 1). The energy harvesting element in this method is essentially a photovoltaic (PV) cell that can directly drive the implanted electronics or recharge its battery, if any. The research presented in this paper has been specifically designed to provide both the required theoretical and experimental results for validating the method. Furthermore, it aimed to discover the advantages as well as the disadvantages of this method and compare it with the other competing techniques.

In Section II of this paper, the basic theory and formulations of optical power delivery is discussed. In Section III, the experimental results and implementation of a PV-driven implanted CMOS chip are presented. The conclusion and discussion come in Section IV.

Sahar Ayazian and Arjang Hassibi are with ECE Department of the University of Texas at Austin, Austin, TX,78712 USA (e-mail: ayaz@mail.utexas.edu and arjang@mail.utexas.edu).

II. Optical Power Delivery

Tissue in general is known to be an absorbing and scattering medium for light [12]. Due to the various structural components that tissue has, it cannot be considered as a homogeneous medium obeying Beer-Lambert Law. However, to simplify the required calculations of light-tissue interactions, a specific tissue type (muscle, liver, skin, fat and etc.) is generally modeled as a homogeneous medium with specific absorption (μ_a) and scattering (μ_s) coefficient. In that case, $T(\lambda)$, the optical transmittance at a specific wavelength (λ), defined as the portion of the optical power that passes through the tissue ($I(\lambda)$), can be approximated by

$$T(\lambda) = e^{-\mu(\lambda)x}, \quad (1)$$

where $\mu(\lambda)$ is the total attenuation coefficient describing both the absorption and scattering phenomena such that

$$\mu(\lambda) = \mu_a(\lambda) + \mu_s(\lambda), \quad (2)$$

and x is the thickness of that layer. Now, if there is a tissue stack that consists of k dissimilar layers with different thicknesses, the overall transmittance, $T_\Sigma(\lambda)$, can be formulated by

$$T_\Sigma(\lambda) = \prod_{i=1}^{k} T_i(\lambda) = e^{-\sum_{i=1}^{k} \mu_i(\lambda) x_i}, \quad (3)$$

where index i corresponds to the characteristics of the i^{th} tissue layer.

To compute the harvested *in-vivo* current, one needs to also know the incident optical power density on the tissue stack, $I_0(\lambda)$, and the responsivity of the implanted PV cell, $R(\lambda)$. If these values are known, then the short-circuit current generated in the PV cell with surface area A, denoted by I_{sc}, becomes

$$I_{sc} = A \int_{\lambda=0}^{\infty} I_0(\lambda) T_\Sigma(\lambda) R(\lambda) d\lambda. \quad (4)$$

The value of I_{sc} can subsequently be used to estimate the available power according to the I-V curve of the PV cell.

III. Implementation and Measurement Results

A. Tissue Characteristics

In Fig. 2A, the measured optical loss (i.e. $-10\log T(\lambda)$) for various types of animal tissue is reported. The tissues used in this experiment are grinded prior to putting them into the spectrophotometer to ensure maximized scattering loss and basically measure the worst-case optical loss. These results support the widely known fact that photons with λ below 700nm and above 2μm have little penetration depth in tissue ($T(\lambda) \to 0$ in these regions) [13]. However, within these wavelengths, generally referred to as the *therapeutic window*, $T(\lambda)$ is non-zero and some portion of the light can in fact penetrate deeper into the tissue. As shown in Fig. 2B, the unique absorption characteristics of water and Hemoglobin (main constituents of the soft tissue) are responsible for this phenomenon. The data from Fig. 2A and (3) suggest that -40dB is the minimum expected loss at λ = 700nm for subcutaneous applications (i.e., device below skin and 1 mm fat) and as one goes deeper into the tissue an approximately 17dB extra attenuation should be added per mm.

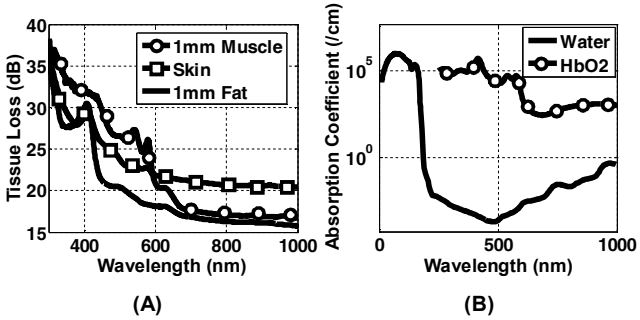

Fig. 2. (A) Measured tissue optical loss and (B) absorption coefficient of water (/cm) [14] and HbO2 (/cmM) [15].

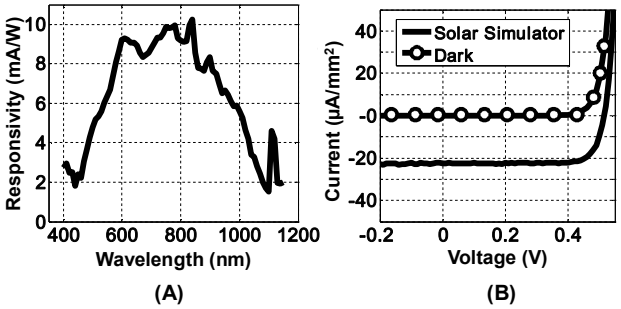

Fig. 3. (A) Measured responsivity of the CMOS P+/N_{WELL} PV cell, and (B) its I-V characteristics in absence and presence of light.

B. PV Cells

In Fig. 3A, the measured $R(\lambda)$ for an implemented silicon-based complementary metal-oxide-semiconductor (CMOS) P+/N_{WELL} PV cell is shown. There are two justifications for using this particular device for optical power delivery. The first is that silicon has a relatively high responsivity in the visible and near IR range which incidentally overlaps with the *therapeutic window*. The second is that CMOS is the fabrication process by which most integrated circuits are built. Hence, by implementing its already-available PV cells, one can monolithically integrate the energy harvesting elements with all the necessary electronics for implanted applications. This not only simplifies the design and fabrication steps, but also significantly lowers the manufacturing costs.

The measured I-V curve of the CMOS P+/N_{WELL} PV cells is shown in Fig. 3B. The curve is identical to the I-V curve of P+/N_{WELL} diode, except that in the PV mode the whole curve is shifted down by I_{sc}. As evident, I_{sc} in the presence of a solar emulator source (Newport, US) is approximately 22μA/mm^2. When no light is present (*i.e.*, the chip is covered), this current drops to below 0.2nA/mm^2. The open-

circuit voltage in the PV mode, V_{oc}, generally remains between 0.4V-0.5V.

By considering the tissue optical loss and the results of Fig. 3A and Fig. 3B, it can be inferred that it is quite feasible to produce 0.1μAs of PV current in bright light conditions (e.g., 1 mW/mm^2 in sunlight) using mm-scale implanted CMOS PV cells. While this current (and power level) is small, it is sufficient to run low-power electronics or slowly recharge an implanted battery [16-17]. In Table I, a specification comparison between the proposed method here and other existing methods is shown. As evident, the advantages of optical power delivery are its simplicity and MRI-compatibility. The main disadvantage is that the power delivery efficiency can become very small for deep implants.

TABLE I
SPECIFICATION COMPARISON FOR POWER DELIVERY

Parameter	Battery	Inductive Coupling	RF Powering	PV
Min. size	1-10 cm^3	1-10 cm^2	1-5 cm^2	1 mm^2
Tissue loss	N/A	Negligible [18]	2dB/mm [11]	20dB/mm
External source	NA	AC source	RF source	Light source
MRI comp.	Yes/No	No	No	Yes
Power density	0.1μW /mm^3	0.8 mW /mm^2 [19]	12μW /mm^2 [10]	0.1μW[1] /mm^2

[1] 1kW/m^2 light (sunlight) and 40 dB optical tissue loss for 0.5V V_{OC}

C. IC Implementation

As a proof of concept, a model implanted sensor with integrated PV-cells has been designed and fabricated using the TSMC 180nm CMOS process. The basic architecture of this CMOS implantable sensor which measures an *in-vivo* resistor or capacitor is illustrated in Fig. 4 and its die micrograph is shown in Fig. 5. The basic function of this chip is to create a frequency-shift keying (FSK) output signal that alternates between f_S and f_R, a transducer-dependant frequency and the reference frequency, respectively. f_S and f_R, and FSK clock frequency, f_{CLK}, are all generated by ring-oscillators operating in the sub-threshold region that are directly driven by integrated PV cells (D_1 and D_2). For transmitting the measured signal to outside, a neuromorphic technique is used which its design was inspired by electrocardiography (ECG) systems. In this method, the implanted chip mimics the heart muscle by creating a polarizing-depolarizing electrical field (powered by D_3) using a set of electrodes within the tissue that can be sensed by ECG electrodes on the surface of the skin. Details of the circuitry within this low-power sensor have been reported before [20]. Here, the experimental results of optically powering up this system are presented.

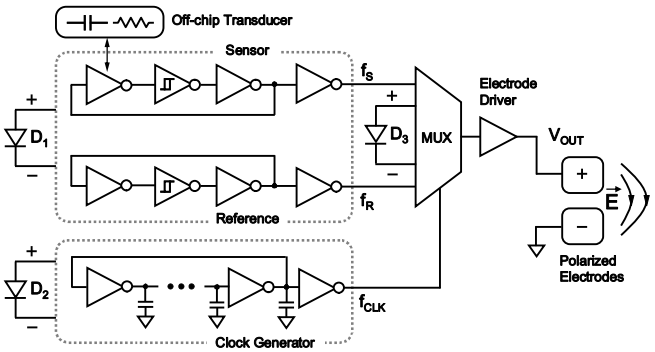

Fig. 4. Architecture of the PV-driven implantable IC.

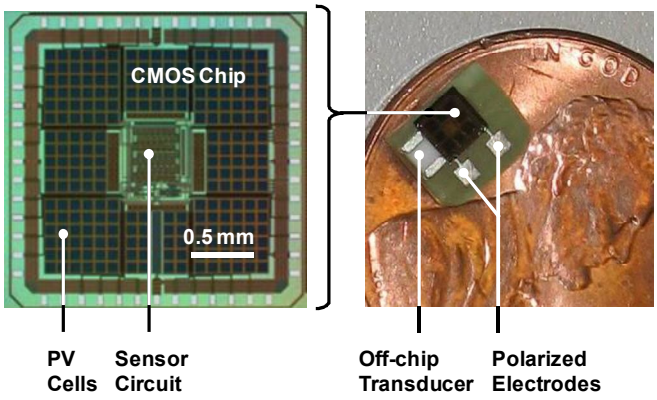

Fig. 5. Die micrograph photo of the implemented CMOS chip.

D. Model-System Measurements

In Fig. 6A the setup for *in-vitro* measurements is shown where the animal tissue model (3 mm bovine muscle and chicken skin) were used to emulate the actual *in-vivo* application. Fig. 6B, shows the setup for estimating the coupling coefficient of the subcutaneous electrode pair with the external ECG electrodes. The ECG electrodes are placed on top of the tissue and the polarized electrodes are beneath it.

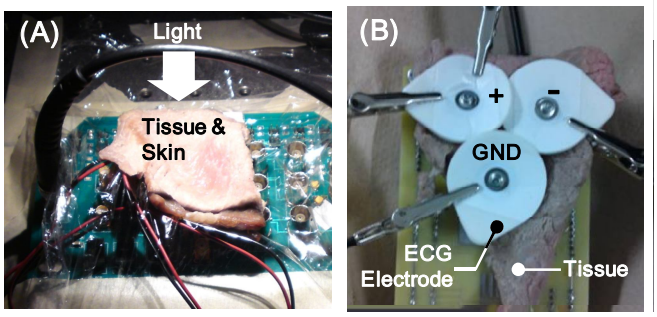

Fig. 6. Setups for (A) *in-vitro* measurements and (B) evaluating subcutaneous-to-surface electrode coupling.

In Fig. 7, the measured sensor transfer functions for measuring *in-vitro* resistance and capacitance are reported. Based on this data, at 2.5 klux, $\Delta f = f_R - f_S$ has a sensitivity of approximately 600 Hz/pF and 390 Hz/MΩ for capacitance and resistance sensing modes, respectively.

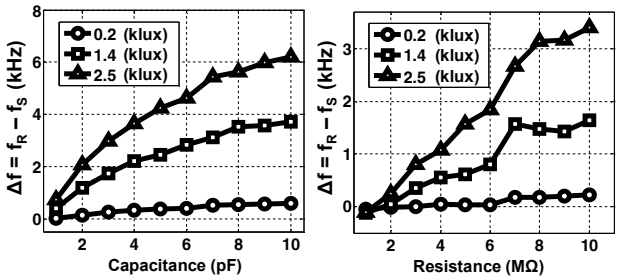

Fig. 7. Implantable sensor oscillation characteristics.

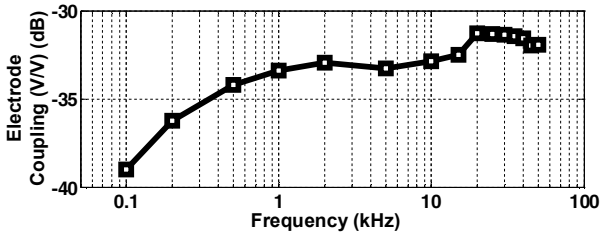

Fig. 8. ECG electrode to implanted electrode measured coupling.

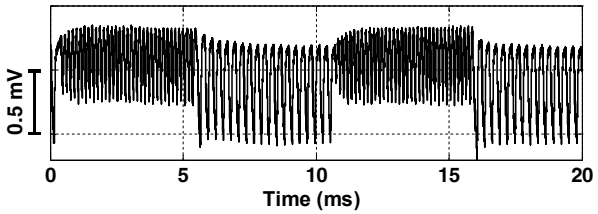

Fig. 9. Measured FSK output signal at 15klux ambient light.

The coupling of the subcutaneous electrode pair with the external ECG electrodes was measured to be approximately -35dB V/V within the 0.1 to 20 kHz range (see Fig. 8). Fig. 9, shows the measured output FSK signal of the chip when measuring a 10pF *in-vitro* capacitor at the ambient light of approximately 15 klux. This result, considering the mV-range amplitude at the output of the CMOS chip, suggests that we are able to produce 10-100 µV FSK signals on the skin. This value is well within the detection range of ECG systems.

IV. Conclusion

Optical power delivery to implanted devices is feasible, easy-to-use, and MRI-compatible. The amount of power is a function of location of the implanted chip and the characteristics of the tissue layers covering it. However, for subcutaneous devices, the optical loss can be as low as 40dB which makes it possible to harvest µW's of power in bright ambient light conditions. This amount of power is small, but enough for low-power applications. The implant does not have to be exposed to light continuously but depending on the application, it should be exposed to light for specific periods of time to store enough energy. This method of powering can be applied in any low power application where the device depth is a couple of mm's.

V. Acknowledgment

The authors want to thank Semiconductor Research Corporation (SRC) and Taiwan Semiconductor Manufacturing Company (TSMC) for supporting this research.

VI. References

[1] Oesterle *et al.*, "New Interfaces to the Body through Implantable System Integration," ISSCC Tech Digest, 2011.

[2] Leung A. M., Ko W. H., Spear T. M., and Bettice J. A., "Intracranial pressure telemetry system using semicustom integrated circuits," IEEE Trans. Biomed. Eng., vol. BME-33, pp. 386–395, Apr. 1986.

[3] Dorman M. G., Prisbe M. A., and Meindl J. D., "A monolithic signal processor for a neurophysiological telemetry system," IEEE. J. Solid-State Circuits, vol. SC-20, pp. 1185–1193, Dec. 1985.

[4] Zoll, P. M., Frank, H. A., Zarsky, L. R. N., Linenthal, A. J. and Belgard, A. H., "Long-term electric stimulation of the heart for Stokes-Adams disease," Ann. Surg., 154: 330,196l.

[5] Akin T., Najafi K., and Bradley R. M., "A wireless implantable multichannel digital neural recording system for a micromachined sieve electrode," IEEE J. Solid-State Circuits, vol. 33, no. 1, pp. 109–118, Jan. 1998.

[6] Smith B., Peckham P. H., Keith M. W., and Roscoe D. D., "An externally powered, multichannel, implantable stimulator for versatile control of paralyzed muscle," IEEE Trans. Biomed. Eng., vol. BME-34, pp. 499–508, July 1987.

[7] Allen H. V., Knutti J. W., and Meindl J. D., "Integrated power controllers and RF data transmitters for totally implantable telemetry," Biotelemetry Patient Monit., vol. 6, pp. 147–159, 1979.

[8] Galbraith D. C., "An implantable multichannel neural stimulator," Ph.D. dissertation, Stanford Univ., Stanford, CA, Dec. 1984.

[9] Yang L., Chow E. Y., Irazoqui P. P., Chappell W., "RF Powering for Embedded Glaucoma Sensors in Miniature Packages," Proceedings of the URSI General Assembly, Chicago, IL (Aug, 2008).

[10] Kurup, D., Joseph, W., Vermeeren, G. and Martens L., "Path-Loss Model for In-Body Communication in Homogeneous Human Muscle Tissue," Electronics Letters, vol. 45(9), pp. 453 - 454, April 2009.

[11] Yuce, M. R.,W. P. Ng, S., Myo, N. L., Khan, J. Y., Liu, W., "Wireless Body Sensor Network Using Medical Implant Band," Journal of Medical Systems, vol. 31(6).

[12] Welch, A. J. and Van Gemert, A. J. C., *Optical-Thermal Response of Laser-Irradiated Tissue*, Plenum Press, New York, 1995.

[13] Konig K., "Multiphoton Microscopy in Life Sciences," Journal of Microscopy, vol. 200(2), pp. 83-104, Nov. 2000.

[14] Segelstein, D. J., "The complex refractive index of water," University of Missouri-Kansas City, (1981).

[15] Prahl, S. (http://omlc.ogi.edu/spectra/hemoglobin/summary.html)

[16] Chen, G. et. al, "Millimeter-Scale Nearly Perpetual Sensor for System Stacked Battery and Solar Cells," ISSCC Dig. Tech. Papers, 288-9, Feb. 2010.

[17] Mark, M., Chen, Y., Sutardja, C., Tang, C., Gowda, S., Wagner, M., Werthimer, D. and Rabaey, J., "A 1mm^3 2Mbps 330fJ/b Transponder for Implanted Neural Sensors," *to appear* in VLSI Circuits Symposium 2011.

[18] Stephenson et al., "Energy Transport through Tissue by Inductive Coupling," The American Journal of Surgery Volume 114, Issue 1, July 1967, Pages 87-94.

[19] Ghovanloo, M. *et al*., "A Wide-Band Power-Efficient Inductive Wireless Link for Implantable Microelectronic Devices Using Multiple Carriers" IEEE Trans. CAS I, vol. 54(10), pp. 2211 - 2221, Oct. 2007.

[20] Ayazian, S., Soenen, E., Hassibi, A.," A Photovoltaic-Driven and Energy-Autonomous CMOS Implantable Sensor," *to appear* in VLSI Circuits Symposium 2011.